Optimised Design of Nested Circular Tube Energy Absorbers under Lateral Impact Loading.

A.G. Olabi[a],*, E. Morris[a], M.S.J. Hashmi[a], and M.D. Gilchrist[b]

* Email: abdul.olabi@dcu.ie

a School of Mechanical and Manufacturing Engineering, Dublin City University, Glasnevin, Dublin 9, Ireland.
b School of Electrical, Electronic and Mechanical Engineering, University College Dublin, Belfield, Dublin 4, Ireland.

Abstract.

Arrangements of mild steel (DIN 2393) nested tubes were laterally crushed by dynamic loading. The tests were performed with impact velocities ranging between 3 and 5 m/s, using a fixed mass impinging onto the specimens under the influence of gravity. Two arrangements of nested tube systems were considered; one standard and one optimised design. Their crushing behaviour and energy absorption capabilities were analysed experimentally and simulated numerically using the explicit code LS-DYNA. Results from the numerical analyses were compared against those obtained from experiments. An over-prediction in force-deflection responses was obtained from the numerical code. An attempt was made to explain this inconsistency on the basis of the validity of strain rate parameters used in the Cowper Symonds relation. It was shown that the optimised energy absorber exhibited a more desirable force-deflection response than the standard arrangement due to a simple design modification which involved mild steel cylindrical dampers.

Nomenclature.

CIPSS Circular In Plane Standard System

CIPDS Circular In Plane Damped System

$\dot{\varepsilon}$ Strain rate

σ_d Dynamic yield stress.

σ_s Static yield stress

D, q Strain rate parameters (Cowper-Symonds relation)

E_{kin} kinetic energy

E_{int} internal energy

E_{si} sliding energy (friction energy)

E_{rw} rigid wall energy

E_{damp} damping energy

E_{hg} hourglass energy

E_{kin}^{0} Initial kinetic energy

E_{int}^{0} Initial internal energy

E_{ext} External work done

1.0 Introduction.

The function of an energy absorber is to absorb kinetic energy upon impact and dissipate it in some other form of energy, ideally in an irreversible manner. Non-recoverable (inelastic) energy can exist in various forms such as plastic deformation, viscous energy and friction or fracture energy in both metallic and composite structures [1, 2, 3]. Circular or square sectioned tubes are among the most commonly used structural elements due to their prevalent occurrence and easy manufacturability. Circular tubes, for example, can dissipate elastic and inelastic energy through different modes of deformation, resulting in different energy absorption responses. Such methods of deformation include lateral compression, lateral indentation, axial crushing, tube splitting and tube inversion. It is important to study their energy absorption characteristics and mean crushing loads so as to determine their applicability to practical energy absorption situations. Such practical cases may consist of energy absorbers in the aircraft, automobile and spacecraft industries, nuclear reactors, steel silos and tanks for the safe transportation of solids and liquids.

Energy absorption through material deformation has been extensively studied over the last three decades, particularly in the form of tubular systems. The lateral compression of a single circular tube and its strain hardening phenomena have been analysed both experimentally and analytically by various authors such as Burton and Craig [4], DeRuntz and Hodge [5], and Redwood [6]. These authors were among the first to analyse such problems and each one of them proposed a slightly different deformation mechanism for the compression of a tube between rigid flat platens. The effect of strain hardening was further examined by Reid and Reddy [7] who developed a theoretical model based on a rigid linear strain hardening material model which appears to be the most accurate one to date. The authors improved the strain hardening prediction by replacing the localised hinges with an arc in which its length changes with deflection. Hence this theoretical model accounts for both the geometric and material strain hardening effect. An important dimensionless parameter which they developed governs the shape of the force-deflection curve. This parameter was defined as 'mR' and is a function of the yield stress in tension, the mean radius R of the tube, the strain hardening modulus E_p and the thickness t. According to Reid and Reddy it may be possible to maximise the energy absorbing capacity by choosing appropriate tube dimensions such that the 'mR' value is minimised since this is a function of tube geometry. Avalle and Goglio [8] examined the strain field generated during the lateral compression of aluminium tubes and proceeded to verify the known theoretical models. Of the three known theoretical models proposed by the various authors [4, 5, 6], it was found that the latter accounted for all the main features observed experimentally, hence this model seems the most realistic in describing the actual

behaviour of the tube both qualitatively and quantitatively. Reddy and Reid [9] proposed a method to calculate a more realistic force-deflection curve using a rigid linear work hardening material model. These tubes were also compressed laterally between rigid platens. It was suggested that an average value of strain hardening modulus could be used to calculate the parameter *'mR'*, therefore these two parameters would be considered constant throughout the deflection range. However, it has been further proposed that if the variation of strain hardening modulus with strain is known, this could be used to update *'mR'* at each load step or load increment and thus obtain a more realistic load-deflection characteristic. It was suggested that the method described above could be used as a basis for obtaining some of the material properties from a ring compression test. Gupta et al [10] conducted a comprehensive experimental and computational investigation of circular metallic tubes subjected to quasi-static lateral loading. Specimens analysed consisted of both mild steel and aluminium tubes with different diameter to thickness ratios. Their corresponding force-deflection responses were obtained and examined in detail. An in depth description was provided on the deformation mechanism of a tube compressed between flat rigid platens.

Nested systems in the form of a line of rings subjected to end impact loading were examined by Reid and Reddy [11]. The authors were principally concerned with identifying the main mechanism which controls the deformation of such systems. Upon experimentation, the main parameters were identified and varied, thereby leading to a suggestion for the construction of a mathematical model of the system. It was found that in low speed impact testing on tube systems, the effect of inertia was secondary; therefore the design of energy absorbing systems could be achieved provided that the material strain rate was taken into account. Reddy et al [12] described experiments in which a variety of one dimensional systems with free distal ends, as opposed to fixed ends, were subjected to lateral impact by a rigid projectile. An elastic–plastic structural shock wave theory, which employs a bilinear material model to describe the collapse behaviour of the rings, was used to analyse the deformation of typical ring chain systems.

A nested system in the form of orthogonal layers of aluminium and mild steel tubes under static lateral compression was investigated by Johnson et al [13]. Such an orthogonal layer consists of a row of tubes stacked upon each other with every second row rotated 90 degrees. The authors concluded that nested ductile tube systems play an important part in producing a monotonic load-deflection response and that the systems which exhibit cracks after loading only induce oscillations into the response and do not produce catastrophic failure in the system as a whole.

A nested system analysed by Shrive et al [14] consisted of two concentric rings with a layer of smaller tubes between them, the axis of all tubes being parallel. Tack welding was used to attach the rings to the concentric tubes. It was found that increases in system stiffness, maximum load and energy absorption was apparent as the level of tack welding increased. From the impact loading experiment, it was found that full deformation did not occur but maximum opposing forces similar to the quasi-static case were achieved.

Reddy and Reid [15] examined the quasi-static lateral compression of a tube constrained so that its horizontal diameter was prevented from increasing. This was a way of increasing the specific energy absorption capacity of the tube by introducing more plastic hinges into the structure. Also the relationship between a single tube and a system of tubes with different configurations was investigated. It was found that the energy absorbed by a closed system (side constraints) was three times more than that of an open system (no constraints); however the maximum deflection of the former was less than that of an open system. Overall it can be concluded that the introduction of side constraints and creating a closed system is a feasible method of increasing its energy absorbing efficiency.

Morris et al [16] analysed the quasi-static lateral compression of nested tube systems between rigid platens both experimentally and numerically. These energy absorbers consisted of both two and three tube systems which were assembled 'In Plane'. Such a term describes two or more tubes of varying diameter being placed within each other and their axes being parallel. This type of energy absorber was compressed under flat rigid platens at a velocity of 3mm/min to ensure no dynamic effects were present. It was demonstrated how such a system is well suited to applications where space or volume restrictions are an important design consideration without compromising energy absorbing requirements.

Morris et al [17] also analysed the post collapse response of nested tube systems with side constraints. This work showed how the introduction of external constraints allows a greater volume of material within the structure to deform plastically in the post collapse stage of compression, thereby absorbing more energy. Nested systems consist of 'short tubes' of varying diameter placed within each other with an eccentric configuration. A related work [18] modified the 'In Plane' system by rotating the central tube 90 degrees to define an 'Out of Plane System'. In doing so, the force-deflection response changed from a non-monotonically increasing response to one that increased monotonically without sacrificing its energy absorbing capabilities. The quasi-static lateral compression was achieved using three different devices such as flat rigid platens, cylindrical and point-load indenters and their corresponding force-deflection response were compared.

Morris et al [19] also studied nested tubes crushed laterally between rigid platens at two different velocities. The first category of energy absorber consisted of an 'In Plane' system; the second device consisted of an 'Out of Plane' system. The material used was cold finished mild steel. The Cowper-Symonds relation was used to predict the dynamic yield stress of the rings and this was included in the FE material model.
It can be seen that extensive research has been conducted by the aforementioned authors in the study of both singular tubes and externally stacked nested systems subjected to lateral loading. However it appears that no investigation has been conducted on the dynamic crushing of an internally stacked system in which a cluster of circular tubes are assembled as described by Morris et al [16].Therefore, this paper is an attempt to consider the effectiveness of this new form of nested system as an energy absorber. In addition, the paper demonstrates how such systems can be optimised so that a desirable force – deflection response can be obtained by introducing a simple mechanism. Experimental analysis of these devices was achieved with the aid of a drop weight impact tester. The loading and response was analysed via the finite element method and the predicted force-deflection response was compared against that measured experimentally.

2.0 Experimental Set-up.

2.1 High Speed Camera.

A high speed video recording system namely the MOTIONSCOPE PCI 2000 S series was used to capture each impact event. The camera head is a 2 ½ * 2 ½ * 4 inch enclosure which contains the CCD sensor. Up to 2000 fps (frame per seconds) of the impact event can be recorded. Video playbacks of 2000 fps in forward and reverse directions are also possible with frame by frame or freeze frame options available. The exposure of each frame is reduced at the higher frame rates, so more light exposure is required as the frame rate increases. Therefore, a specialised lighting system was employed to increase illumination. The video files are in Microsoft avi (audio video interleaved) format by default; however they can be converted to jpeg with resolutions of up to 480*420 pixels.

2.2 Mechanical Features of the Impact Tester.

A Kistler 9091 series piezoelectric force transducer was used to capture the load-time response of the impact events. This transducer has a large dynamic range and good frequency response of 160,000 samples/sec. Maximum load magnitudes of up to 250kN are possible. The transducer is placed in the moving carriage and connected to the striker via a lock-unlock mechanism. The complete moving mass consisting of both the

carriage and striker is allowed to drop vertically between two vertical parallel guide rails from a maximum height of 1.2 metres.

A photo gate arrangement consisting of photo diodes which pass through a flagged gate was used to capture the initial velocity of the striker just before impact.

2.3 Data Acquisition System.

The data acquisition system Rosand IFW (Intelligent Free Wheel) V 1.10 was used to capture the signals from the force transducer. The maximum sampling rate is 670 kHz. The software gathers the force measurements with respect to time, the frequency of which is dependent on sweep time and number of data points selected. If the signal filter is used, the data is then shown with a filter applied but this can be applied or removed retrospectively as raw data is always stored. The type of filter used is based on the second order Butterworth filter, implemented in the software as an IIR (infinite impulse response), i.e., a recursive filter.

2.4 Material Properties.

The tubes used in this work were made of mild steel which was cold finished, drawn over mandrel by the manufacturer according to DIN standards (DIN 2393 ST 37.2) and containing approximately 0.15% carbon. Between five and seven dog bone samples for each of the three different sized tubes were analysed in order to ensure consistent results. The dog bone samples were machined from cut-out specimens obtained from the acquired tube stock. The true static stress-strain curve was obtained using a tensile test based on ASTM standards. The stress - strain curves obtained from the samples displayed highly unusual behaviour in which strain softening occurred almost immediately after yielding with no apparent sign of any strain hardening which is not consistent with normal behaviour of mild steel. Therefore, it was decided to approximate the material property of the three tubes using a bilinear stress-strain curve. In doing so, the yield stress of 470MPa was carefully obtained from the experimental stress-strain curve at 0.2% strain. A non-zero value of 1500 MPa for the plastic modulus was assigned to represent the plastic portion of the stress-strain curve. The stated plastic modulus is validated from [20]. The yield stress is validated according to DIN standards which claim the yield stress of this material to be within the range of 450 MPa to 525MPa.

3.0 Experimental Work.

3.1 The Preparation Stages.

For impact testing of the samples, a Zwick Roell version 5HV was employed, as shown in Fig. 1a. A custom made fixture was designed and manufactured to hold the samples relative to the impinging striker, as shown in Fig. 1b. It should be noted that such a fixture will automatically prevent the full displacement stroke from being achieved; approximately 5mm of a displacement stroke is lost. A total of 11 samples were tested, as shown in Table 1. This table displays their corresponding initial velocity, final velocity, impact duration, displacement and energy absorbed. For clarity, Fig. 1c illustrates a schematic of both the circular in-plane standard system (CIPSS) and the damped systems (CIPDS) compressed dynamically under a flat rigid platen. When testing each sample, the impinging mass was kept at a constant value of 34.7kg. This total mass consisted of both the striker and the carriage. The machine allows the user to select either velocity, drop height or energy absorption to set the striker in motion. The latter of these was used and hence the corresponding velocity and drop height were calculated by the machine software. The velocity time response of each sample was summed and averaged and is shown in Fig. 2. The length of the energy absorbers varied from 10mm to 15mm, the latter value being the upper limit due to the energy capacity restrictions of the machine. Prior to each test being conducted on each sample, the drop height parameter was set to zero before specifying an energy absorption value. This was done by adjusting the striker to just touch the tip of each sample. Once the energy absorption value was specified, the machine automatically adjusted the striker to its appropriate height. For each sample tested, the data from the transducer was collected at a frequency of 5000Hz and a total of 100 data points were collected (i.e. 20ms time interval). The video recorder was mounted on a tripod and adjusted until a good viewing range was obtained. In order to improve the quality of the video image, a black contrasting neutral material was placed behind the samples.

4.0 Experimental Results and Discussion.

4.1 Analysis of the Circular In-Plane Standard System (CIPSS).

Fig. 3 shows the various responses and photographic evolutions of a CIPSS compressed under dynamic loading conditions. Five specimens were tested to represent this type of absorber. As illustrated in Fig. 3a, the response from each sample was reasonably consistent. For this system there was an initial gap of approximately 18.9mm between the outer and central tubes and 18.9mm between the central and inner tubes. These two gaps allowed all three components to deform sequentially as loading proceeds, hence the reason for the non-monotonic rise in force throughout the deformation stroke. Fig. 3b depicts sample 5 in its filtered

and unfiltered state, the former was used subsequently for comparison purposes against numerical results at a later stage in this work. Since the force time response was consistent, it can be seen that the input velocity applied to each sample. Fig. 3c was also consistent indicating that the striker was raised to its correct height for each test. Upon examination of Fig. 3d, there was an increase in the rate of energy absorption as each tube was compressed in succession, reaching a final value of approximately 225J. The digital photographs (Fig. 3e) display the evolution of this energy absorber as recorded by the high speed video recorder with each image displaying the time of contact in milliseconds.

4.2. Analysis of the Circular In-Plane Damped System (CIPDS).

The experimental output responses of a CIPDS are shown in Fig. 4. In an attempt to achieve a smoother force-deflection response than that exhibited by a CIPSS (Fig. 3a), two cylindrical spacers were inserted between the tubes as illustrated in Fig. 4e. From this, it can be clearly seen that once the moving mass impinges on this absorber, the three tube components will begin to deform synchronously. It should be noted that in order for the spacers to remain in position during the displacement stroke and to maintain symmetry, a mild steel dowel was placed through the machined holes of the upper portions of the tubes and the two spacers. A spot weld was used to fuse both ends of the dowel to the absorber. The placement of the cylindrical spacers inserted between the gaps of the tubes serves two purposes: firstly, to dampen out the abrupt rise in force as contact is established between the tubes as deformation proceeds, and secondly to reduce the rate of strain hardening due to the radius of curvature of the spacers. This reduction in strain hardening was demonstrated by Shim and Stronge [21], who analysed the lateral crushing of thin walled tubes using cylindrical indenters and side constraints. A complete range of indenter radii were used varying from zero curvature (flat platens) to infinite radius (point load indenters) to crush these thin walled tubes and to examine their responses. It was discovered that, depending on the radius of curvature of the indenters, the post collapse behaviour of laterally compressed tubes can be either stable (deformation-hardening) or unstable (deformation-softening). Therefore, in this work, the radius of curvature of the spacers inserted between the three tubes can be seen as an intermediate condition between the limiting cases of a flat plate and point load-indenter. This marks a force-deflection response that was approximately rectangular in shape as shown in Fig. 4a. Examining the displacement-time response of this system (see Fig. 4c), samples 6 and 7 show final displacements of approximately 45mm each whilst the remaining samples exhibited higher values. This was due to the fact that samples 6 and 7 were tested first but only with limited energy. The energy input was increased for the remaining samples in order to achieve full displacement stroke before ‘bottoming out’

occurred. The energy time curve (see Fig. 4d) exhibits a more linear response than that of a CIPSS but with a slight decrease in energy absorption in the later stages of the impact event. Fig. 4e. shows the physical evolution of sample 8 with the inclusion of the cylindrical spacers.

5.0. Development and Analysis of the Finite Element Models.

5.1 Finite Element Modelling.

The explicit non linear finite element code LS-DYNA was used to predict the response of the aforementioned energy absorbers subjected to a free falling impinging mass. The complete model consisted principally of the striker, the assemblage of tubes and the base. These three components were modelled with an explicit structural solid element consisting of eight nodes having translations, velocities and accelerations in the x, y and z directions at each node. The striker was modelled as a rigid entity with a translational displacement permitted in the vertical y direction, all other rotations and translations being fixed. In the material model, the mass density was increased to represent the total mass of both the carriage and striker. For each of the two different absorbers analysed experimentally, an average velocity time curve was obtained and applied to the striker for the four different modelling cases. The base was modelled as rigid with all rotations and translations defined as fixed entities. The tubes contained within the two various energy absorbers were discretized by full integration solid elements. Although this type of formulation leads to an increase in CPU time, the undesirable feature of hour glassing was avoided.

5.2. Mesh Convergence.

A mesh convergence analysis was performed in order to ensure a sufficient mesh density was used to accurately capture the deformation process. Fig. 5 illustrates the convergence plot of three different mesh densities. It can be seen that a convergent solution was achieved when three or five elements were used to mesh the thickness of the tubes. Hence all subsequent models consisted of a mesh density involving three elements through the thickness of each tube as represented by the inlay illustration in Fig. 5. The algorithm used to simulate contact between the respective components (striker, tubes and base) was based on the ‘AUTOMATIC SURFACE TO SURFACE CONTACT’ in which contact is established when a surface of one body penetrates the surface of another body. A static coefficient of friction value of 0.2 was assigned to the contact pairs to prevent lateral movement between the respective tubes.

5.3. Material Characterisation.

For material characterisation of the tubes, a bilinear stress–strain curve was incorporated into the finite element model using the 'PLASTIC KINEMATIC HARDENING' material model option. Values of 0.3 and 200 GPa were given for Poisson's ratio and Young's modulus respectively. The material is assumed to possess only isotropic strain hardening and strain rate effects due to dynamic loading as defined using the Cowper-Symonds constitutive equation given by

$$\sigma_d = \sigma_s \left(1 + \left[\frac{\dot{\varepsilon}}{D} \right]^{\frac{1}{q}} \right) \tag{1}$$

where σ_d is the dynamic flow stress at a uniaxial plastic strain rate $\dot{\varepsilon}$, σ_s is the associated static flow stress, the material constants given for D and q were 6844 and 3.91 respectively. These values were used in previous studies for the axial crushing of mild steel tubes and dynamic loading [22]. The values for the yield stress and plastic modulus, as outlined in Section 2.4, were incorporated into this material model.

6.0. Numerical Results and Discussion.

6.1. Energy Balance.

To ensure that there were no numerical errors within the developed models to simulate the various energy absorbers, the energy equation was checked to ensure that it was in a balanced state. The following energy equation must hold true at all times during an analysis and is given by [23] -

$$E_{kin} + E_{\text{int}} + E_{si} + E_{rw} + E_{damp} + E_{hg} = E^0_{kin} + E^0_{\text{int}} + E_{ext}$$

Where, on the left hand side, E_{kin} is the kinetic energy, E_{int} the internal energy, E_{si} the sliding energy (friction energy), E_{rw} rigid wall energy, E_{damp} is energy due to damping and E_{hg} is hourglass energy; on the right hand side, $E^0_{kin}, E^0_{\text{int}}, E_{ext}$ are energies due to initial kinetic, initial internal and external work done respectively. Since the models in question only contain kinetic, internal and sliding energy and external work done on the system, the energy balance reduces to

$$E_{kin} + E_{\text{int}} + E_{si} = E_{ext}$$

The terms on the left hand side are equivalent to the total energy. Hence, it can be seen from Fig. 6b and Fig. 7b that the energy condition for each model was in a balanced state, indicating that no energy was introduced or absorbed artificially that may be generated due to numerical instability.

6.2. Evaluation of the CIPSS.

Fig. 6a and Fig. 6d shows the force - and energy - time responses for a CIPSS simulated using the explicit numerical method and its comparison to that of experiments. Upon examination of the former curve, it appears that contact between each of the respective tubes was predicted to occur at slightly different times by both the experimental and numerical methods. For example, the time of contact between the outer tube and central tubes predicted by the numerical method occurs at approximately 4ms as opposed to a shorter time of 3ms observed in experiments. Contact between the central tube and the inner tube are predicted by the experimental and numerical methods, to occur at approximately 6ms and 8ms respectively. One possible explanation for the different times of contact between the experimentally observed and numerically predicted results may be linked to the behaviour of the clamp as shown in Fig. 1b. Initially, the system containing the three tubes is clamped tightly into the base plate prior to impact. However, as the striker impinges onto the outer tube, the bottom portion of the outer tube begins to flatten out, thereby causing the central and inner tube to loosen momentarily until contact is re-established between each respective tube. Similarly, as the central tube is plastically compressed, the bottom portion of same will also straighten out, causing the inner tube to momentarily loosen. If it is arbitrarily assumed that the central tube loosened by 5mm inside the clamp with the striker travelling at precisely 4.58m/s (striking velocity for the CIPSS as shown in Fig. 2.), this would result in a significant time difference of 1.1ms. By examining the CIPDS system in Fig. 7a, it can be seen that the contact time between the two methods is identical. This is for the reason that the cylindrical spacers within this CIPDS cause all three tubes to be displaced at the same time and hence there is no momentary loosening of the system under the clamp. In relation to the CIPSS, it can be seen that for the striker to traverse 18.9mm (distance between the outer and central tube, see Fig. 1c) at a velocity of 4.58m/s requires a time of 4.1ms, since the time taken is the distance traversed divided by the velocity. Additionally, for the striker to traverse a total distance 37.8mm (distance between the outer, central and inner tube respectively, see Fig. 1c) requires a time of 8.2ms. These two results appear to be in good agreement with the contact times illustrated by the numerical code as shown by the arrows in Fig. 6a. This would suggest that some loosening occurred with the CIPSS inside the clamp during the displacement stroke and thereby causing a time disparity between the numerical and experimental results.

The energy - time response appears to display good agreement between both methods. The evolution displacement plots extracted from the numerical method are displayed in Fig. 6e. It appears that one can be confident that the deformation mode response is in good agreement with that of experiments (see Fig. 3e). The displacement - time curve shows good agreement between the two methods, which is to be expected since an average velocity time curve pertinent to each absorber was applied to the striker. The same holds true for the remaining energy absorber as shown in Fig. 7c.

6.3. Evaluation of the CIPDS.

Fig. 7a and Fig. 7c depicts the force - and energy - time response of a CIPDS. There appears to be a significant over prediction in force magnitude displayed by the numerical method. A 15% over prediction in energy absorption was observed for this energy absorber. In order to explain this discrepancy of results, Fig. 8 was created. Upon analysis of the CIPDS (see Fig. 8), it can be seen from an experimental point of view that both the static and dynamic cases exhibit similar force deflection response in terms of magnitude. This would indicate that, for the given velocity applied to the striker, that the strain rate sensitivity is not a significant factor in the deformation response of this particular system. Also, with the advantage of using the numerical model to demonstrate the effect of strain rate insensitivity by excluding the strain rate parameters, it can be seen that numerical results agree favourably with both the static and dynamic experimental cases. This would appear to signify that the values of D and q used in the Cowper-Symonds relation may not be valid in this particular application of energy absorbers since an obvious large increase in the dynamic yield stress is evident using the specified strain rate parameters. The usual constants of 40.4 and 5 for D and q are normally used by researchers; however, it was found that substitution of these values into the Cowper-Symond relation yields an even larger value of yield stress than the constants of 6844 and 3.91 used in the current material model (see Section 5.3).

The constants of 40.4 and 5 also have been used by [24] to predict the dynamic force magnitude for the internal inversion of mild steel tubes. It was found that the dynamic load conditions greatly over-predicted those that were recorded experimentally. It appears that the constants only apply to applications involving small strains (5%) and not to large strains that are encountered in the internal inversion of mild steel tubes. Large strains also exist in the lateral compression of the aforementioned tube systems with both the CIPSS and CIPDS systems experiencing an effective plastic strain value of approximately 16%. Therefore, it appears that more research needs to be conducted in this area, specifically to obtain experimental data pertaining to material strain rate sensitivity of mild steel. Such experimental data needs to be collected in the

form of a range of constants which represent the behaviour of mild steel at different strain rates and strain levels [25]. A lack of such experimental data may be due to the difficulty of conducting controlled dynamic tests at large strains. The accessibility of such information would help assist in the analysis of the effects of strain rate on the force magnitude of the various systems compressed dynamically in this work. The availability of the dynamic yield stress (normalised by the static yield stress) as a function of strain rate for the material used in this work would enable us to determine the correct constants D and q by curve fitting the result to the Cowper-Symonds relation. In doing so, the dynamic force -deflection response from the numerical model analysed with these constants should match up closely with the dynamic response as obtained in experiment.

It can be hypothesised, however, that the constants D and q may be indirectly estimated calculated by obtaining a response of dynamic yield stress as a function of strain rate via the numerical method. This relation would be obtained based on the dynamic force deflection response (strain rate excluded) which fits the experimental data well as shown in Fig. 8. If this is possible, the constants obtained as a result of this hypothesis may be confirmed by comparison with the availability of dynamic yield stress – strain rate experimental data. Fig. 9. illustrates a force – time response for the CIPDS with two different sets of parameters D and q. The first set of values was used in all the numerical models in this work and used in previous studies as outlined in section 5.3. The second set of values was chosen arbitrarily with parameter D left constant and q reduced to a value of 1.5. It can be seen how choosing this value of q marks a response that compares well to the experimentally measured one. One could conclude that if such experimental data pertaining to strain sensitivity was available, the value of q may well indeed lie in the region of 1.5 and thereby would illustrate good agreement with the experimentally observed CIPDS force – time response as shown in Fig. 9.

It should be noted that the strengthening influence of strain rate on the flow stress of mild steel is a maximum at small strains and decreases as the plastic strain increases, as observed by Campbell and Cooper [26]. Reid and Reddy [27] studied the effects of strain rate on the dynamic lateral compression of mild steel tubes. They discovered that the strain rate of a single tube of 50mm diameter was $22.5s^{-1}$ when compressed dynamically at 5m/s. The CIPSS and CIPDS systems were also subjected to an initial dynamic loading velocity in the region of 5m/s, as illustrated in Fig. 2. However, the dimensions of the present tubes were larger than that analysed by Reid and Reddy, ranging from 95mm O.D. to 127mm O.D. According to the numerical model of the CIPDS, a mean strain rate value of $23s^{-1}$ was obtained indicating the similarity in results as observed by

the same authors. In the discussion of strain rates, it is usually the order of magnitude which is of significance. Hence, the dynamic systems analysed in this work are at the lower end of the 'Low Dynamic' spectrum as illustrated by [28]. The upper and lower range of strain rates pertaining to this spectrum is in the region of $10s^{-1}$and $10^{3}s^{-1}$ thus indicating that strain rate effects of the two systems are at a minimum and hence, the dynamic yield stress will be at a minimum.

7.0. Conclusion.

An experimental program has been reported describing the procedure in setting up an impact tester for the dynamic lateral compression of two types of circular energy absorbers, namely the CIPSS and CIPDS. An explanation was given on how the insertion of a simple damping mechanism interacts with the tubes to exhibit a desirable force-deflection response. Concurrent to the experimental work, results of the explicit non-linear finite element method using LS-DYNA to simulate the dynamic crushing of the various absorbers was presented. The boundary conditions of the numerical models were subjected to the same test conditions observed in the experimental program. An attempt was made to explain why large discrepancies existed between the experimental and numerical methods for the CIPDS. It is believed that this is due to the lack of suitable physical data of the Cowper-Symonds constants at large strains for the mild steel material used in this work. A numerical energy balance was examined on each model to ensure that no artificial energy was introduced: this confirmed that no numerical errors were associated with these analyses. Despite the over-predictions exhibited from the numerical code, an optimised force deflection response was obtained. The optimised energy absorber (CIPDS) is seen as an improvement on the CIPSS since the insertion of cylindrical damping rods cause the crushing force to be constant once the collapse load has been reached, which is a desirable feature in the design of energy absorbers.

(a)

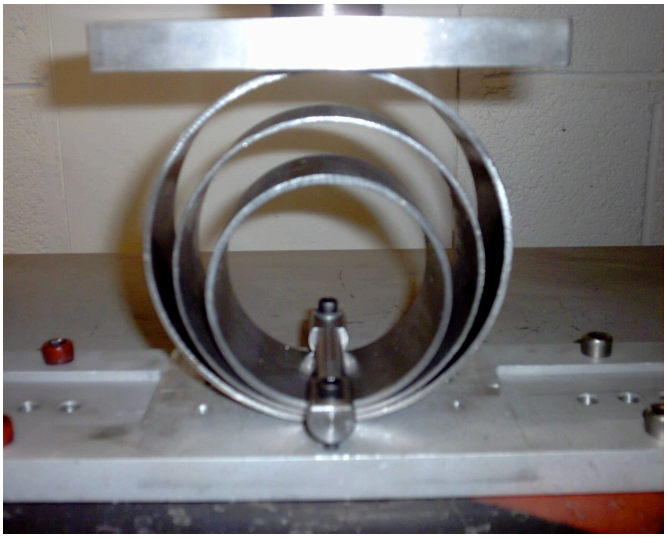

(b)

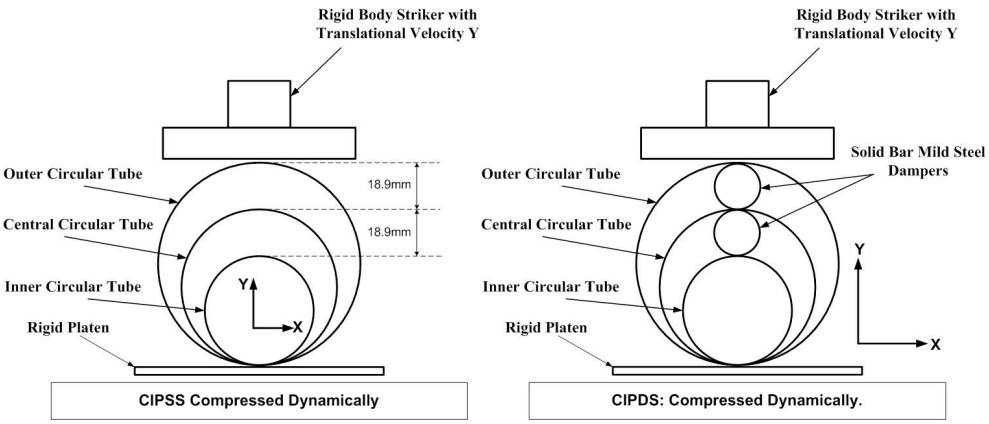

(c)

Fig. 1 (a) The Zwick Roell impact machine used to conduct the experiments.
(b) The fixture used to hold the samples in place upon impact.
(c) A schematic showing both the CIPSS and the CIPDS compressed dynamically.

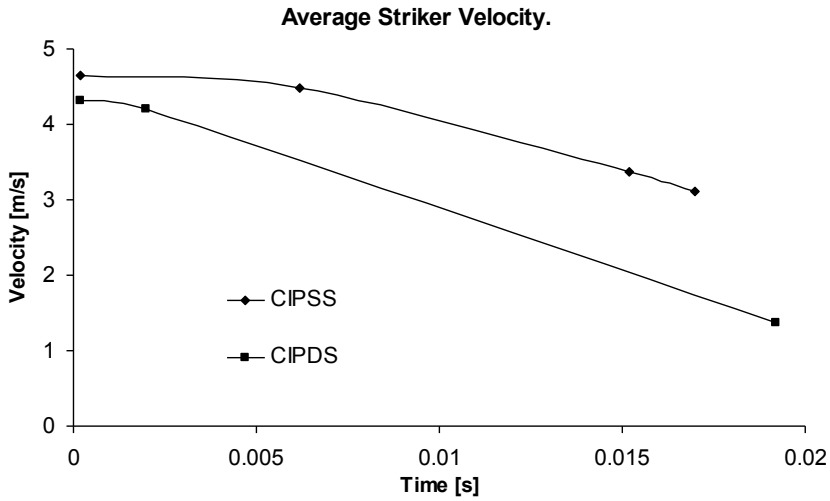

Fig. 2. The average striker velocity applied to the respective samples.

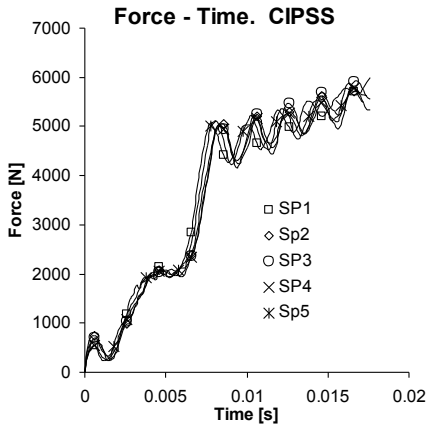

(a)

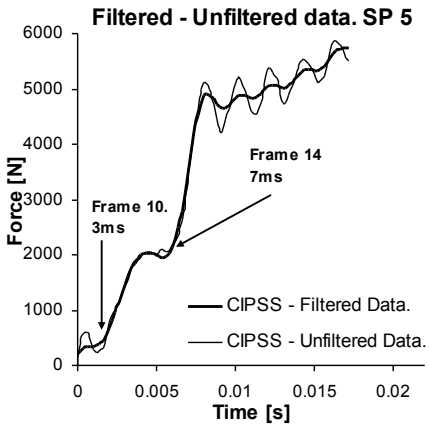

(b)

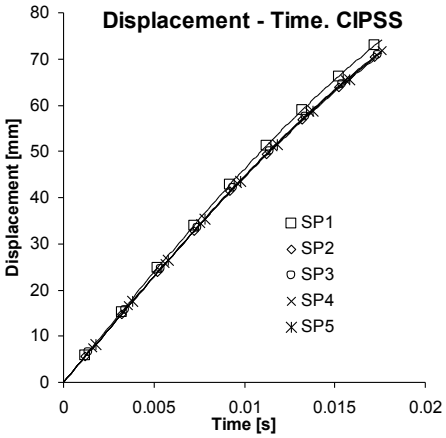

(c)

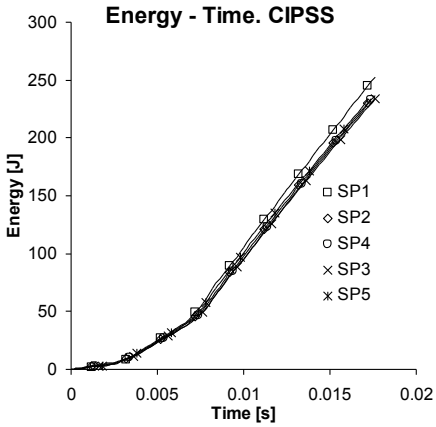

(d)

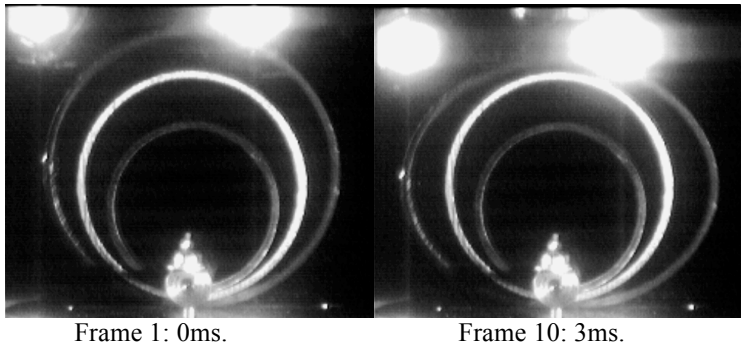

Frame 1: 0ms. Frame 10: 3ms.

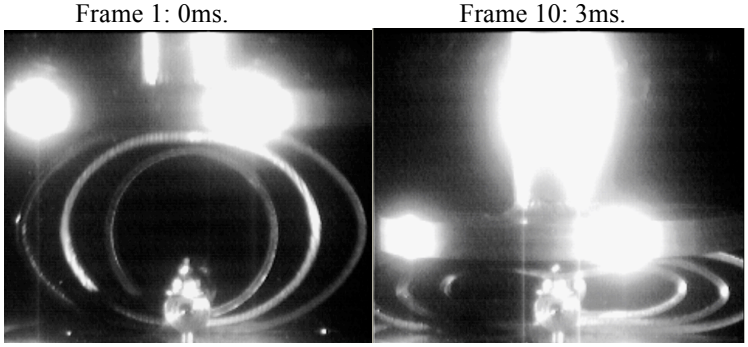

(e) Frame 14: 7ms. Frame 34: 19ms.

Fig. 3. (a) Force time curve for a CIPSS, (b) Sample 5: Filtered-unfiltered data, (c) Displacement time curve for a CIPSS, (d) Energy time response for a CIPSS, (e) Experimental displacement evolution of sample 5.

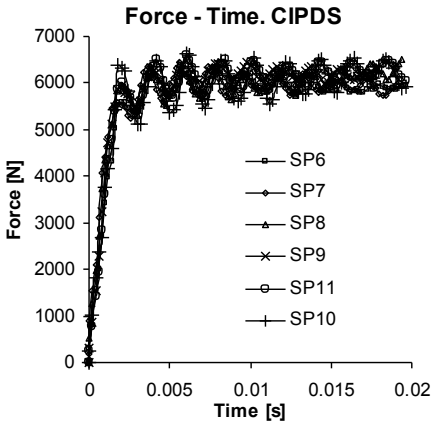

(a)

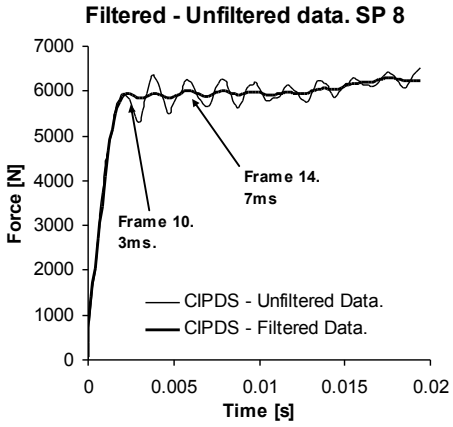

(b)

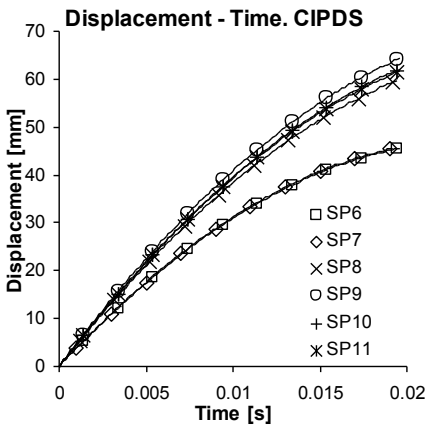

(c)

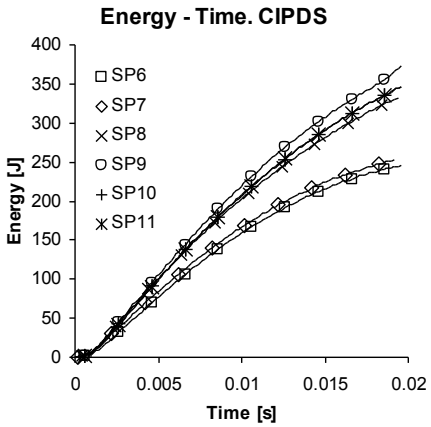

(d)

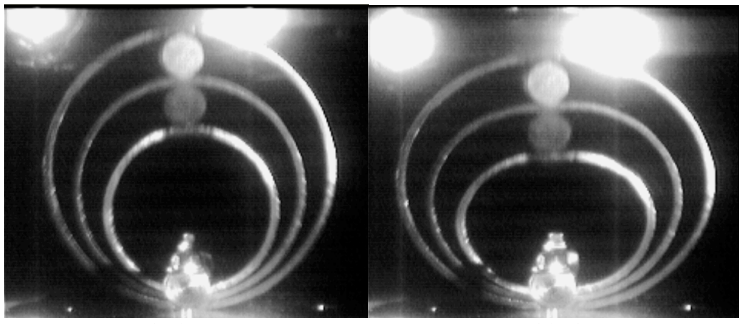

Frame 1: 0ms. Frame 10: 3ms.

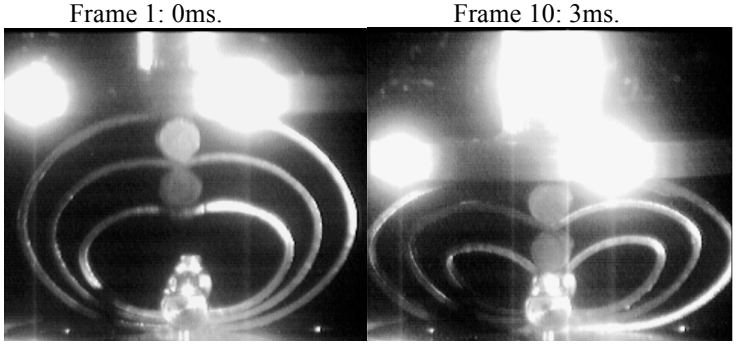

(e) Frame 14: 7ms. Frame 29: 19ms.

Fig. 4. (a) Force time curve for a CIPDS, (b) Sample 8: Filtered-unfiltered data, (c) Displacement time curve for a CIPDS, (d) Energy time response for a CIPDS, (e) Experimental displacement evolution of sample 8.

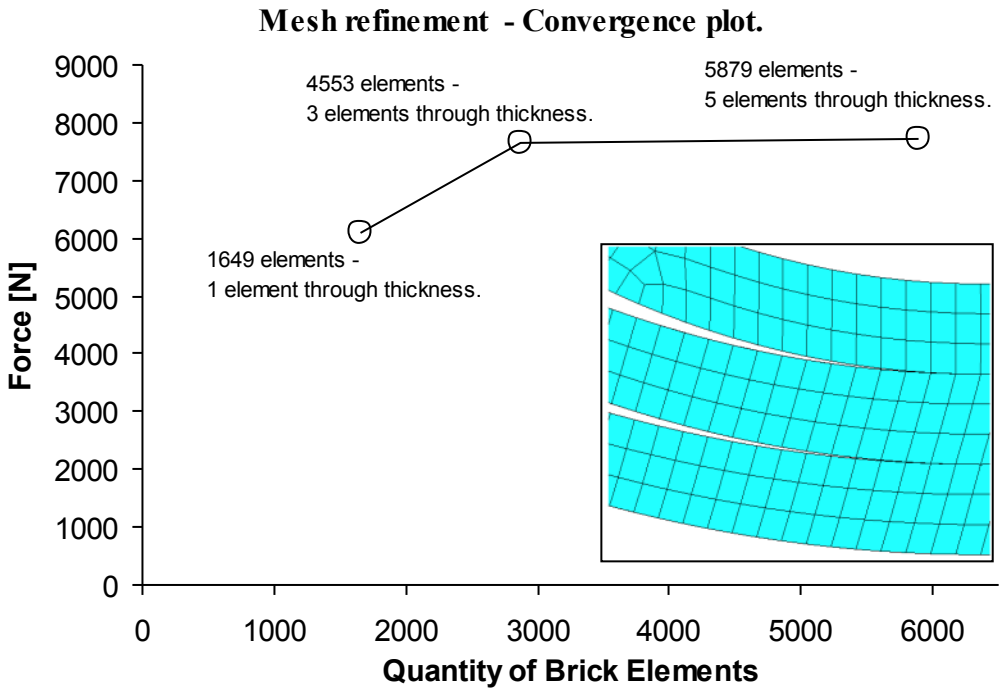

Fig. 5. A force convergence plot of 3 different mesh densities.

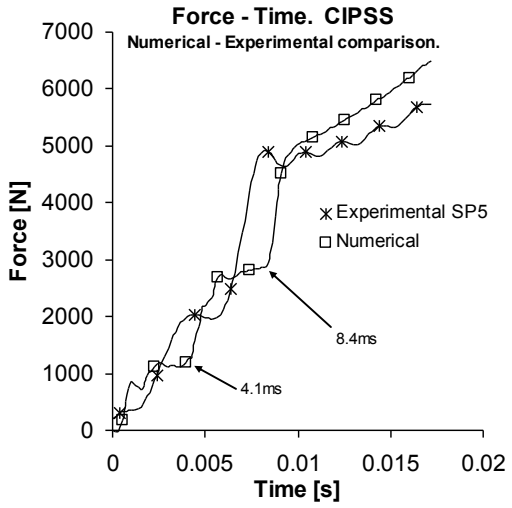

(a)

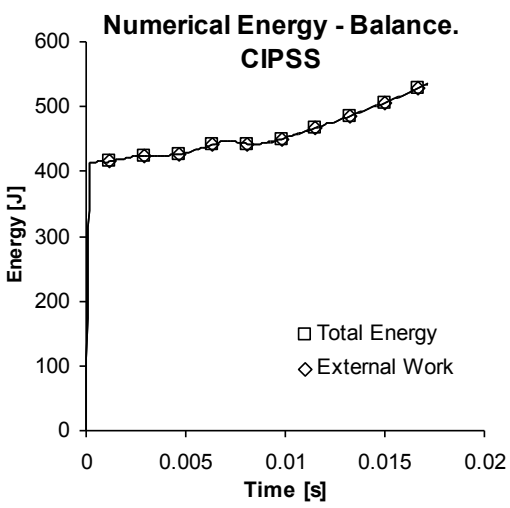

(b)

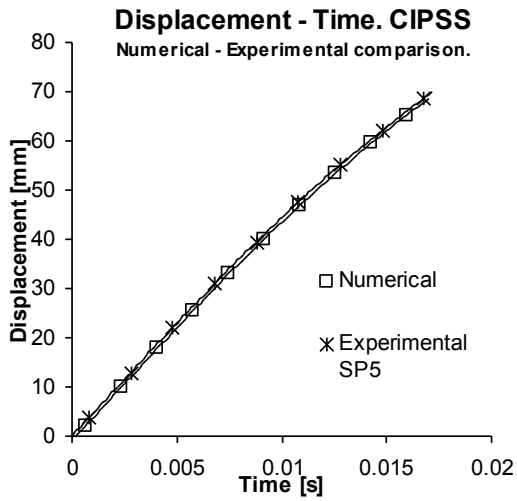

(c)

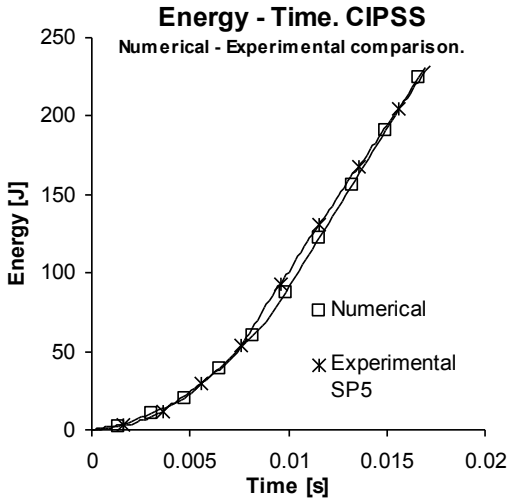

(d)

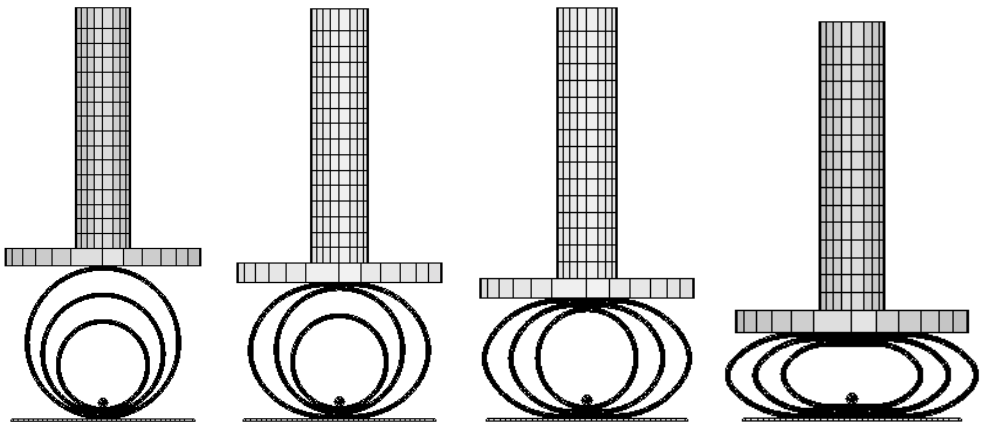

(e)

Fig. 6. (a) Force time curve for a CIPSS. Numerical and experimental comparison, (b) Numerical energy balance, (c) Displacement time curve for a CIPSS. Numerical and experimental comparison, (d) Energy time response for a CIPSS, Numerical and experimental comparison, (e) Numerical plot of displacement evolution for a CIPSS.

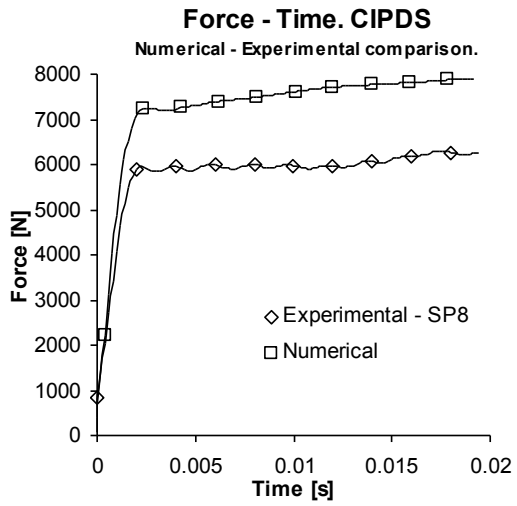

(a)

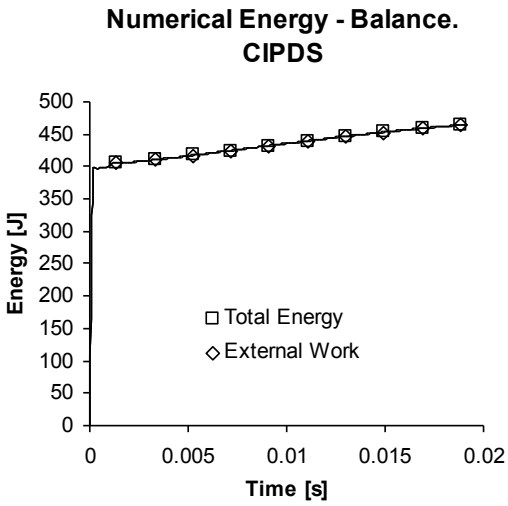

(b)

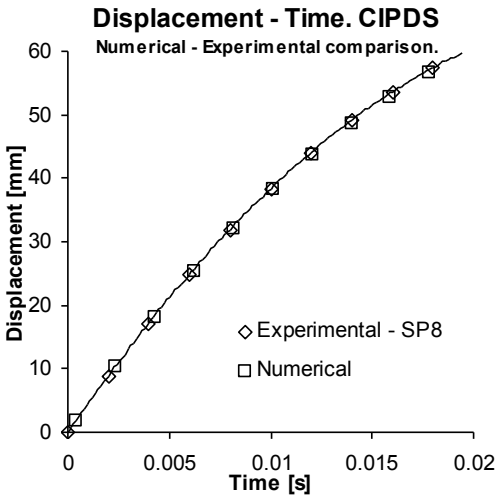

(c)

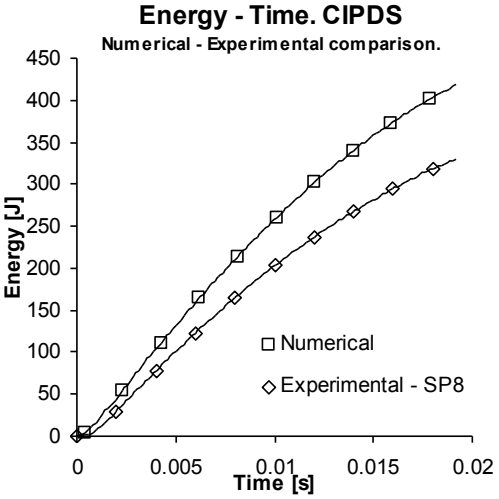

(d)

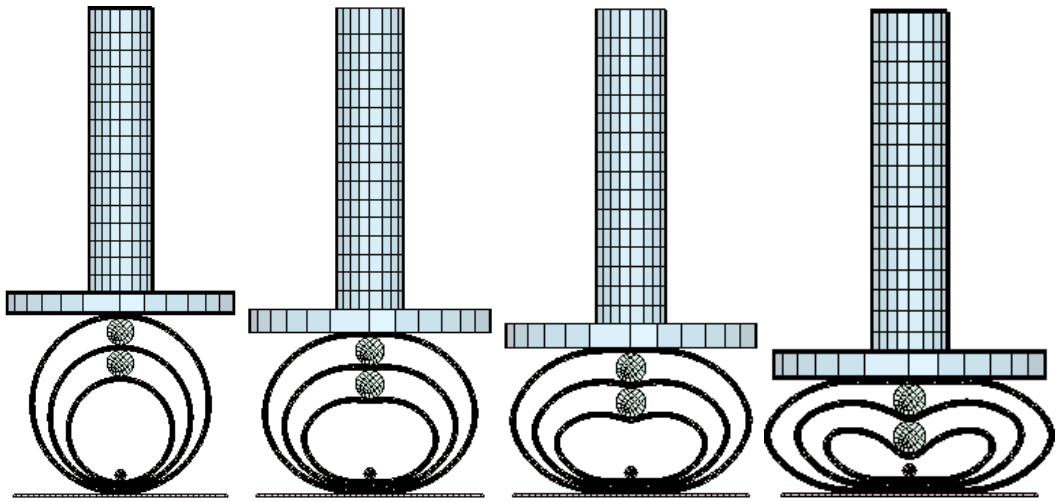

(e)

Fig. 7. (a) Force time curve for a CIPDS. Numerical and experimental comparison, (b) Numerical energy balance, (c) Displacement time curve for a CIPDS. Numerical and experimental comparison, (d) Energy time response for a CIPDS, Numerical and experimental comparison, (e) Numerical plot of displacement evolution for a CIPDS.

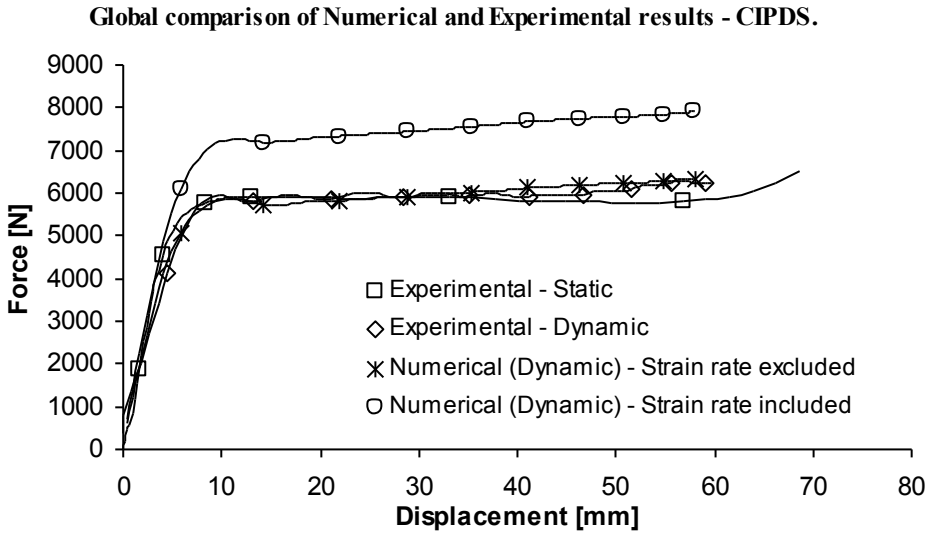

Fig. 8. **Comparison of results for a CIPDS. Static and dynamic cases.**

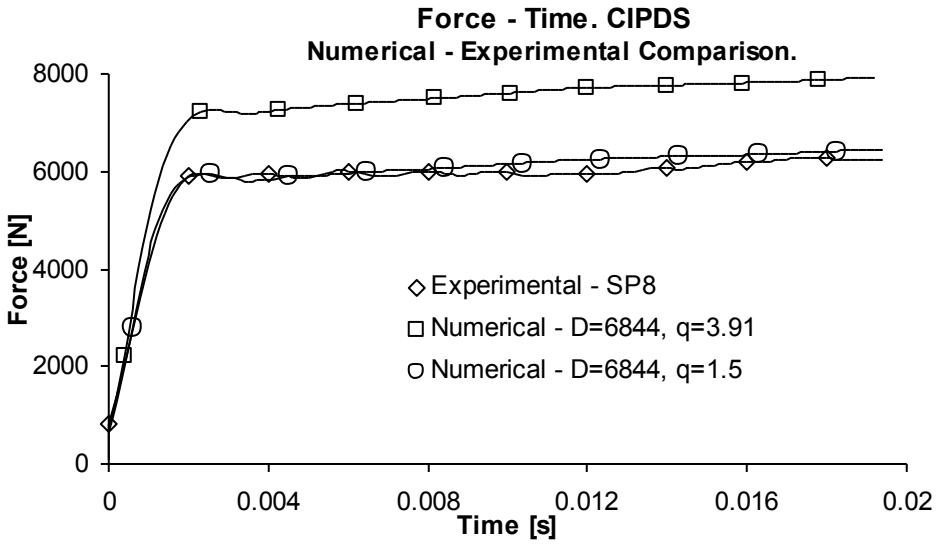

Fig. 9. Force – time response of a CIPDS: The effect of changing the parameter q and leaving D constant.

Table 1. Results obtained from experiments for the 11 samples tested.

	T_{final} (s)	$V_{initial}$ (mm/s)	V_{final} (mm/s)	Stroke (mm)	Energy (J)
CIPSS Length (10mm)					
SP1	0.0176	4780	3120	74	252
SP2	0.0174	4610	3030	70	233
SP3	0.0176	4600	2990	71	236
SP4	0.0176	4610	3030	71	233
SP5	0.0172	4600	3020	70	232
CIPDS Length (15mm)					
SP6	0.0196	3720	750	45	246
SP7	0.0192	3780	820	45	252
SP8	0.0194	4490	1480	59	332
SP9	0.0196	4740	1480	64	373
SP10	0.0196	4600	1550	62	346
SP11	0.0196	4580	1500	61	346

References.

[1] Gilchrist, M.D., Kinloch, A.J., Matthews, F.L., Osiyemi, S.O., “Mechanical performance of carbon fibre and glass fibre-reinforced epoxy I-beams: Mechanical behaviour.” Composites Science & Technology, 56 pp. 37-53 (1996).

[2] Svensson, N., Gilchrist, M.D., “Modelling of failure of structural textile composite.” Computational Mechanics, 26 (3), pp. 223-228 (2000)

[3] Gilchrist, M.D., Curley, L., “Manufacturing and ultimate mechanical performance of carbon fibre-reinforced epoxy composite suspension push rods for a formula 1 racing car.” Fatigue & Fracture of Engineering Materials & Structures, 22 (1), pp. 25-32 (1999).

[4] Burton, R.H., Craig, J.M., "An Investigation into the Energy Absorbing Properties of Metal Tubes Loaded in the Transverse Direction. "1963, BSc (Eng) Report, University of Bristol, England.

[5] DeRuntz, J. A., Hodge, P. G., "Crushing of a Tube between Rigid Plates." Transactions of ASME, Journal of Applied Mechanics., 1963, 30:391-395.

[6] Redwood, R. G., "Discussion of Ref. 2." Transactions of ASME, Journal of Applied Mechanics., 1964, 31:357-358.

[7] Reid, S. R., Reddy, T. Y., "Effect of Strain Hardening on the Lateral Compression of Tubes between Rigid Plates. " Int J of Solids and Structures, 1978, 14 (3): 213-225.

[8] Avalle, M., Goglio, L., "Static Lateral Compression of Aluminium Tubes: Strain Gauge Measurements and Discussion of Theoretical Models." Journal of Strain Analysis., 1997, 32 (5):335-343.

[9] Reddy, T., Reid, S., "On Obtaining Material Properties from the Ring Compression Test." Nuclear Engineering and Design, 1979, 52:257-263.

[10] Gupta, N. K., Sekhon, G. S., Gupta, P. K., "Study of Lateral Compression of Round Metallic Tubes." Thin-Walled Structures, 2005, 43(6):895-922.

[11] Reid, S. R., Reddy, T. Y., "Experimental Investigation of Inertia Effects in One- Dimensional Metal Ring Systems Subjected to End Impact -- I. Fixed-Ended Systems," Int J of Impact Engng, 1983, 1(1):85-106.

[12] Reddy, T. Y., Reid, S. R., Barr, R., "Experimental Investigation of Inertia Effects in One-Dimensional Metal Ring Systems Subjected to End Impact--II. Free-Ended Systems," Int J of Impact Engng, 1991, 11(4):463-480.

[13] Johnson, W., Reid, S. R., Reddy, T. Y., "The Compression of Crossed Layers of Thin Tubes." Int J of Mech Sci, 1977, 19(7):423-428.

[14] Shrive, N., Andrews, K., England, G., "The Impact Energy Dissipation of Cylindrical Systems." Structural Impact and Crashworthiness. J. Morton, editor. Elsevier Applied Science Publishers. London, England, 1984. Vol 2: p. 544-554.

[15] Reddy, T., Reid, S., "Lateral Compression of Tubes and Tube-Systems with Side Constraints." Int J Mech Sci, 1979, 21(3): 187-199.

[16] Morris, E., Olabi, A., Hashmi, S., "FE Simulation and Experimentation of Nested Systems under Static and Impact Loading Conditions."In: Proceedings of the 12th International Conference on Experimental Mechanics. Bari, (Italy) 2004. p. 196-203.

[17] Morris, E., Olabi, A., Hashmi, S., "Post Collapse Response of Nested Tube Systems with Side Constraints." In: Vickery, J., editor. Proceedings of the 22nd International Manufacturing Conference. Tallaght, Dublin (Ireland) 2005. p. 693-700.

[18] Morris, E., Olabi, A., Hashmi, S., "Experimental and Numerical Analysis of the Static Lateral Compression of Tube Type Energy Absorbers with Different Indenters." The Engineers Journal, 2005. 59(8) p. 505 - 510.

[19] Morris, E., Olabi, A., Hashmi, S., "Plastic Response of Nested Systems under Static and Dynamic Loading Conditions using FE and Experimental Techniques."In: Dulieu-Barton J., Quinn, S., editors. Proceedings of the 4th International Conference on Advances in Experimental Mechanics. Trans Tech Publications, 2005, Vol 3-4: p 377-382.

[20] Reddy, T. Y., Reid, S. R., "Phenomena Associated with the Crushing of Metal Tubes between Rigid Plates," Int J of Solids and Structures, 1980, 16(6):545-562.

[21] Shim, V. P., Stronge, W. J., "Lateral Crushing of Thin-Walled Tubes between Cylindrical Indenters," Int J of Mech Sci, 1986, 28(10):683-707.

[22] Nagel, G., Thambiratnam, D., "A numerical Study on the Impact Response and Energy Absorption of Tapered Thin-Walled Tubes". Int J of Mech Sci. 2004, 46(2):201-216.

[23] LS-Dyna Theoretical Manual, Livermore Software Technology Corporation: Livermore, California; May 1998.

[24] Harrigan, J. J., Reid, S. R., Peng, C., "Inertia Effects in Impact Energy Absorbing Materials and Structures," Int J of Impact Engng, 1999, 22(9-10):955-979.

[25] Abramowicz, W., Jones, N., "Dynamic Progressive Buckling of Circular and Square Tubes," Int J of Impact Engng, 1986, 4(4):243-270.

[26] Campbell, J.D., Cooper, R.H., "Some comments on the modelling of material properties for dynamic structural plasticity.", Proc. Conf. on Mechanical Properties at High Rates of Strain. The Institute of Physics Conf. Series No. 102., London, pp 77 – 87. (1989).

[27] Reid, S., Reddy, T., "Effects of strain rate on the dynamic lateral compression of tubes." Proc. Conf. on Mechanical Properties at High Rates of Strain. The Institute of Physics Conf. Series No. 47, Ch. 3, pp. 288-298 (1979)

[28] Lu, G., Yu, T., "Energy Absorption of Structures and Materials." Woodhead Publishing Limited, Cambridge, 2003.